

Molybdenum Carbide as Alternative Catalysts to Precious Metals for Highly Selective Reduction of CO₂ to CO**

Marc D. Porosoff, Xiaofang Yang, J. Anibal Boscoboinik, and Jingguang G. Chen*

Abstract: Rising atmospheric CO₂ is expected to have negative effects on the global environment from its role in climate change and ocean acidification. Utilizing CO₂ as a feedstock to make valuable chemicals is potentially more desirable than sequestration. A substantial reduction of CO₂ levels requires a large-scale CO₂ catalytic conversion process, which in turn requires the discovery of low-cost catalysts. Results from the current study demonstrate the feasibility of using the non-precious metal material molybdenum carbide (Mo₂C) as an active and selective catalyst for CO₂ conversion by H₂.

To sustain future population and economic growth, the global energy supply is expected to increase by 60% by 2040,^[1] but the associated CO₂ emissions are a major concern. CO₂ capture and conversion must become a significant industry to mitigate the threat of climate change and ocean acidification.^[2,3] Efforts have already been put forth to capture and sequester CO₂,^[4,5] however, a process that can efficiently convert CO₂ into a commodity chemical has the potential to provide a better solution compared to sequestration.^[6,7] One attractive route is converting CO₂ into CO, which can be used as feedstock in the Fischer–Tropsch process, a well known and well characterized route that has been used in industry to produce chemicals and synthetic fuels from syngas (CO + H₂) for many decades.

Precious metals are the most commonly used catalysts for CO₂ conversion by H₂.^[8,9] It is generally accepted that catalytic conversion of CO₂ by H₂ occurs over precious metal catalysts in two principle steps.^[10] First, metal sites facilitate the dissociation of molecular hydrogen and the

hydrogenation of CO₂ into formate,^[11] then the oxide support assists with the cleavage of the C=O bond. Therefore, this reaction requires a dual functional catalyst that exhibits high activity for both hydrogen dissociation and C=O bond scission. It has been previously shown^[12] that platinum (Pt) based catalysts supported on CeO₂, a reducible oxide, were more active for CO₂ conversion than those supported on γ-Al₂O₃, an irreducible oxide.^[13] However, in an effort to reduce material costs for CO₂ conversion, it is important to minimize or eliminate precious metals in catalysts. This is particularly important for large-scale processes that would be required to substantially reduce CO₂ emissions.

Transition metal carbides (TMCs) are attractive alternatives because they have similar properties to precious metal catalysts in reforming,^[14,15] hydrogenation,^[16] water-gas shift (WGS),^[17,18] and CO oxidation^[19,20] reactions. The high activity of TMCs compared with their parent metals originates from a modification of the electronic properties from the addition of carbon,^[21] which in turn affects the binding energy and the reactivity of adsorbates.^[22] Mo₂C is particularly interesting for CO₂ conversion because of its low cost, dual functionality for H₂ dissociation and C=O bond scission, and potential to behave similarly to reducible oxides.

In CO₂ conversion by H₂, CO is a desired product for its ability to be used in the Fischer–Tropsch process, while CH₄ is undesired because of its low volumetric energy density and abundance.^[23] Thus, modifying Mo₂C with a metal that can dissociate the unwanted product, CH₄, and thereby recarbure the catalyst to maintain its active, carbidic form is highly desirable. Here, we first investigate CO₂ activation over well-defined Mo₂C surfaces with temperature-programmed surface reaction (TPSR) and ambient-pressure X-ray photoelectron spectroscopy (AP-XPS) experiments to confirm the active nature of the Mo₂C surface toward CO₂ conversion to CO. Then, model surface results are extended to flow reactor experiments over porous Mo₂C catalysts, and further explained by in-situ X-ray absorption near edge spectroscopy (XANES) experiments. The findings show that Mo₂C outperforms precious metal bimetallic catalysts and is highly active and selective for CO₂ conversion to CO. The activity, selectivity and stability of Mo₂C can be further improved by modifying the carbide with another metal, cobalt (Co).

The TPSR experiments over a Mo₂C model surface, prepared by carburizing a single-crystal Mo(110) substrate, were conducted using the AP-XPS system at Brookhaven National Laboratory. The TPSR for CO₂ hydrogenation was conducted under 100 mTorr CO₂ and 700 mTorr H₂. Five gas-phase species, *m/e* = 44 (CO₂), 31 (methanol), 28 (CO), 18 (H₂O) and 15 (CH₄), were recorded while the sample was heated to 523 K and then cooled to 373 K. TPSR results for

[*] Prof. Dr. J. G. Chen
Department of Chemical Engineering, Columbia University
500 W. 120th St., New York, NY 10027 (USA)
E-mail: jgchen@columbia.edu

M. D. Porosoff
Department of Chemical and Biomolecular Engineering
University of Delaware
150 Academy St., Newark, DE 19716 (USA)

Dr. X. Yang
Chemistry Department, Brookhaven National Laboratory
2 Center St., Upton, NY 11973 (USA)

Dr. J. A. Boscoboinik
Center for Functional Nanomaterials (CFN)
Brookhaven National Laboratory
2 Center St., Upton, NY 11973 (USA)

[**] The work carried out at BNL Chemistry and CFN was sponsored under Contract No. DE-AC02-98CH10886 with the U.S. Department of Energy, Office of Science, Division of Chemical Sciences.

Supporting information for this article is available on the WWW under <http://dx.doi.org/10.1002/anie.201404109>.

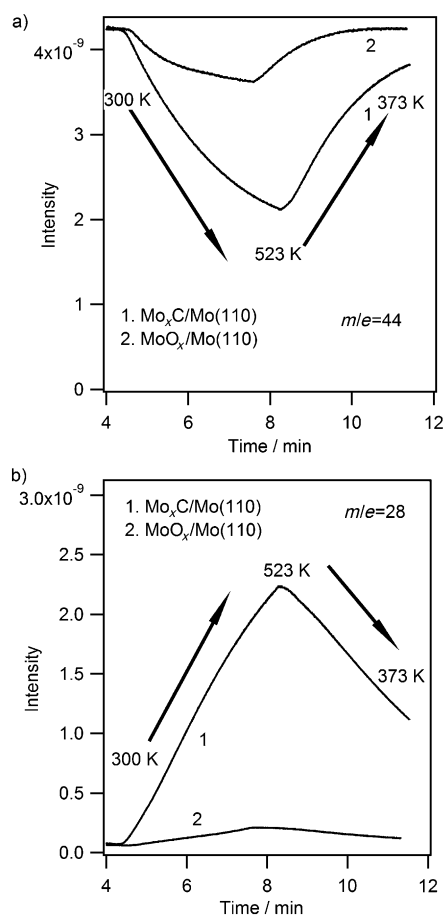


Figure 1. TPRS of CO₂ conversion over 1) Mo₂C/Mo(110) and 2) MoO_x/Mo(110). a) $m/e = 44$, corresponding to consumption of CO₂; b) $m/e = 28$, corresponding to production of CO. TPRS conditions: 100 mTorr CO₂, 700 mTorr H₂.

CO₂ ($m/e = 44$) in Figure 1a show that Mo₂C/Mo(110) is much more active for CO₂ activation than MoO_x/Mo(110). Figure 1b shows the production of CO ($m/e = 28$) from the two surfaces. Comparison of other products is shown in Figure S2 in the Supporting Information. Neither CH₄ ($m/e = 15$) nor methanol ($m/e = 31$) was detected. Thus, the Mo₂C surface is highly selective in converting CO₂ to CO.

AP-XPS investigations of the Mo₂C/Mo(110) surface under CO₂ reduction by H₂ conditions were performed to identify possible surface reaction intermediates. Figure 2 shows the C1s and O1s regions of surface species on Mo₂C/Mo(110) under near-ambient pressures. As seen in Figure 2a-1, evidence for the formation of carbide is shown by the appearance of the C1s peak at 282.9 eV, consistent with the reported value of 282.8 eV.^[24] The O1s peak at 530.4 eV is attributed to the presence of small amounts (ca. 10%) of unreduced MoO_x on the surface. After exposing the surface to 150 mTorr CO₂, the C1s and O1s peaks of gas-phase CO₂ appear at 292.0 and 537.3 eV, respectively. A small peak at 283.6 eV is assigned to oxycarbide (O-Mo-C), in agreement with the reported value of 283.5 eV for molybdenum oxycarbide powder catalysts.^[24] The O1s of oxygen-modified Mo₂C, with the oxygen bonded to carbon, appears at

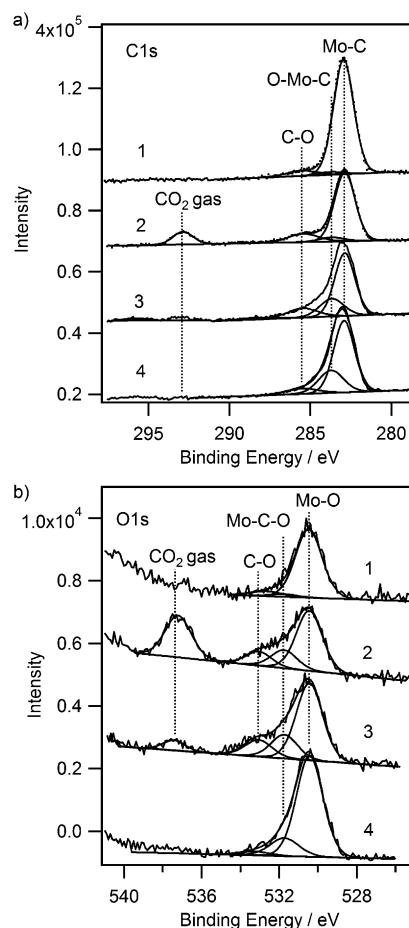


Figure 2. AP-XPS of a) C1s and b) O1s of Mo₂C under various treatment conditions for CO₂ activation. 1) Clean Mo₂C, 2) 150 mTorr CO₂ at room temperature, 3) 150 mTorr CO₂ + 550 mTorr H₂ with annealing to 523 K, then cooling to room temperature, 4) 150 mTorr CO₂ + 550 mTorr H₂ at 523 K.

531.7 eV.^[15] Table S1 in the Supporting Information summarizes the binding energies for both C1s and O1s peaks.

After reaction at 523 K, both C1s and O1s peaks of gas-phase CO₂ are significantly reduced, corresponding to the consumption of CO₂ by reaction. Meanwhile, the C1s peak at 283.6 eV and O1s peak at 531.7 eV increase in intensity, indicating higher coverage of surface oxycarbide after reaction. Figure 2a-4 and b-4 show the AP-XPS results during reaction at 523 K. Under reaction conditions, the major surface species are oxycarbides, indicating the presence of oxygen atoms on the Mo₂C surface during CO₂ reaction contributes to the catalytic activity. Previous studies over oxide-supported metal catalysts have proposed carbonate (CO₃), carboxyl (CO₂^{δ-}) and formate (HCOO) as the reaction intermediates for CO₂ activation.^[25-27] These surface intermediates have been identified by AP-XPS on Cu and CeO_x/Cu(111) surfaces after exposing CO₂ at ambient pressure, with intense C1s peaks for CO₃, CO₂^{δ-} and HCOO located at 289.3, 288.4 and 287.3 eV, respectively.^[24] In comparison, the AP-XPS measurements on Mo₂C in Figure 2 do not show evidence supporting the presence of these intermediates, suggesting a different reaction mecha-

nism for CO₂ activation on Mo₂C. One potential pathway is the direct reaction of CO₂ with Mo₂C to produce CO and oxycarbide (Mo₂C-O), with Mo₂C-O being subsequently reduced by hydrogen to produce H₂O and Mo₂C. This is consistent with the detection of H₂O in the TPSR experiments in Figure S2 and with previous studies of steady-state H₂O production from the hydrodeoxygenation of C₃ oxygenates over Mo₂C.^[28]

Further studies in a flow reactor at 573 K over Mo₂C powder catalysts were carried out to verify the trends seen in the idealized model surfaces. Several precious metal based bimetallic catalysts, demonstrated previously in a batch reactor to be more active for CO₂ conversion than monometallic Pt or Pd,^[12] were also evaluated as references. Experimental information regarding reactor studies and the synthesis and characterization of the catalysts can be found in the Supporting Information. Steady-state reactor results in Figure 3a show that the turnover frequency (TOF) on CeO₂-

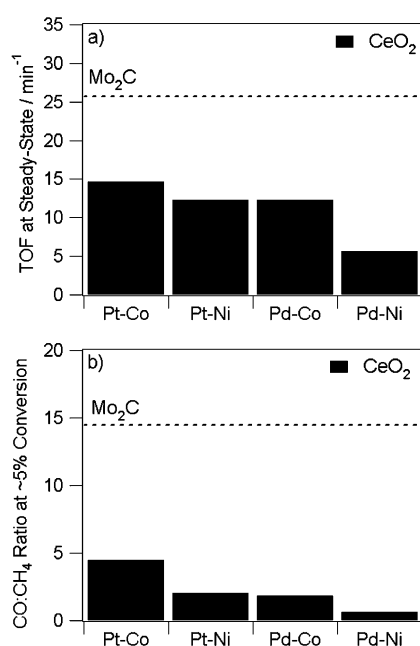


Figure 3. a) TOF and b) selectivity at 573 K on bimetallic supported catalysts on CeO₂ (black bars) and Mo₂C (dashed line).

supported catalysts follows the trend of Pt-Co > Pt-Ni ≈ Pd-Co > Pd-Ni. The conversion of each of the bimetallic catalysts, including monometallic Ni and Co can be found in Figure S7. Although bimetallic catalysts are active for CO₂ reduction, Figure 3 indicates that Mo₂C clearly outperforms them in both activity and selectivity. Specific values for TOF and CO:CH₄ ratio are shown in Table 1. The higher activity of Mo₂C may originate from its direct participation in the reaction through facile oxygen transfer. Upon CO₂ dissociation, an oxygen atom is incorporated into Mo₂C, forming an oxycarbide that can be subsequently reduced by H₂. This process of oxygen transfer is analogous to the role of the reducible oxide in CeO₂-supported bimetallic catalysts.^[12]

Figure 3 shows that bimetallic catalysts containing Co outperform their Ni containing counterparts. Therefore, by

Table 1: Summary of conversion, TOF and selectivity of selected bimetallic catalysts, Mo₂C and 7.5 wt % Co-Mo₂C.

Catalyst	Conversion [%]	TOF [min ⁻¹]	CO:CH ₄ Ratio
PtCo/CeO ₂	6.6	14.6	4.5
PdNi/CeO ₂	2.5	5.6	0.6
Mo ₂ C	8.7	25.7	14.5
Co-Mo ₂ C	9.5	16.1	51.3

combining Co with the highly active Mo₂C catalyst, it is possible to further improve the catalytic performance of Mo₂C. As shown in Table 1, the addition of 7.5 wt % Co to Mo₂C leads to an increase in conversion from 8.7 to 9.5 % while the CO:CH₄ ratio improves from 15 to 51.

In a study by Izhar et al., Co-Mo₂C catalysts dissociate CH₄ into H₂ and C, with amorphous CoMoC_yO_z being identified as the critical active phase that dissociates CH₄.^[29] In the current study, the ability of Co-Mo₂C to dissociate CH₄ is most likely responsible for improving the CO:CH₄ selectivity by reacting with the CH₄ product or CH_x intermediate that leads to CH₄ formation.

Further evidence of the effect of Co on Mo₂C for CO₂ conversion is shown as a function of Co loading in Figure S8. The 7.5 wt % Co-Mo₂C was identified as the optimal catalyst investigated in this study, and stability measurements in a flow reactor were conducted to measure the steady-state conversion and CO:CH₄ ratio of the catalyst. After 36 h on stream, Co-Mo₂C showed improved activity, selectivity, and stability over Mo₂C. The activity and selectivity of Co-Mo₂C were higher than Mo₂C initially and did not decrease over the course of the reaction. Figure S9 contains the comparison of steady-state results of Co-Mo₂C and Mo₂C.

The improved performance of Co-Mo₂C over Mo₂C was likely because the active phase of the catalyst, Mo₂C, was maintained in a carburized state during the reaction, as confirmed by in-situ XANES measurements. Evidence of recarburization of Mo₂C is provided in the Mo₂C/MoO₃ linear fits from XANES spectra of Mo₂C in Table 2, with selected

Table 2: Mo₂C/MoO₃ compositions from linear fits of XANES spectra recorded under various reaction conditions. All reactions performed at 573 K and data collected at room temperature.

Treatment condition	Percent Mo ₂ C [%]	Percent MoO ₃ [%]
Fresh	83.2	16.8
Reduced in H ₂	92.7	7.3
CO ₂	82.7	17.3
CO ₂ + H ₂	91.1	8.9
7.5 wt % Co-Mo ₂ C (Fresh)	29.0	71.0

spectra shown in Figure 4a. The results in Table 2 indicate that a fraction of Mo in Mo₂C can be cycled between reduced and oxidized states. The Mo₂C catalyst cycles between 92.7 % Mo₂C/7.3 % MoO₃ under reduction conditions, then forms a greater amount of oxidized species, likely oxycarbide, when exposed to pure CO₂. With the addition of H₂ to the CO₂ stream at 573 K, some of the oxycarbide is reduced, but the catalyst is not restored to the initial reduced state.

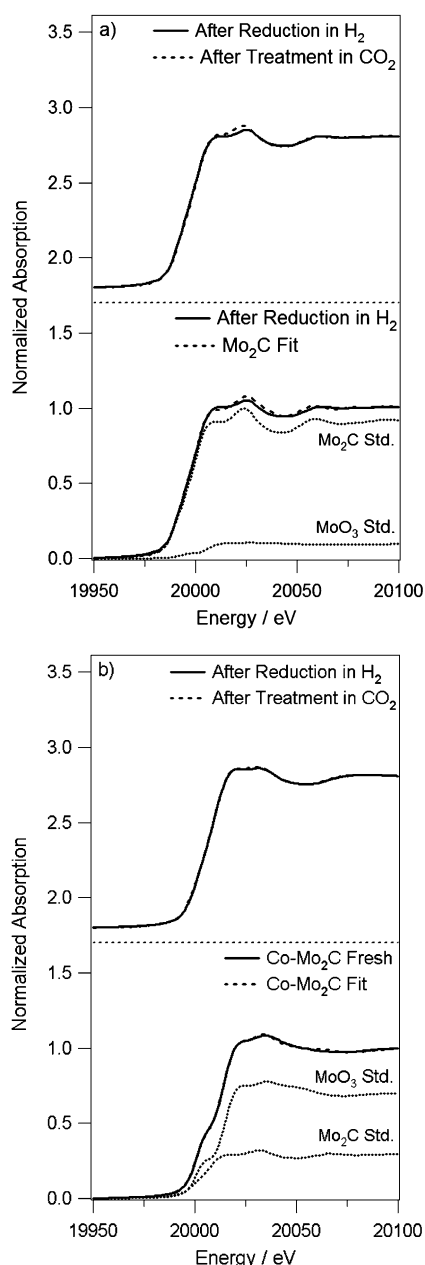


Figure 4. Mo K-edge XANES spectra at room temperature. a) Mo_2C and b) 7.5 wt% $\text{Co-Mo}_2\text{C}$. Top panels show Mo K-edge XANES spectra of samples after reduction, and after treatment in CO_2 . Bottom panels contain linear combination fits with contributions from Mo_2C and MoO_3 standards.

In-situ XANES measurements were also performed on the 7.5 wt% $\text{Co-Mo}_2\text{C}$ catalyst to determine the effect of Co on the oxidation/recarburation cycle. The composition, according to the linear combination fit of the fresh 7.5 wt% $\text{Co-Mo}_2\text{C}$ catalyst was found to be 29.0% Mo_2C /71.0% MoO_3 , a much higher degree of oxidation than the pure Mo_2C (Figure 4b). After further treatments in H_2 , CO_2 , and CO_2/H_2 , the catalyst could no longer be successfully fit by linear combination fit analysis. It is likely that after reduction, a CoMoC_yO_z phase formed, which would explain the inability of a combination of Mo_2C and MoO_3 to accurately represent the catalyst.

Additionally, as seen in Figure 4b, the Mo K-edge of the $\text{Co-Mo}_2\text{C}$ catalyst is virtually unchanged from reduction in H_2 to treatment in CO_2 at 573 K. This lack of change in the oxidation state of Mo in $\text{Co-Mo}_2\text{C}$ is a distinct difference from the pure Mo_2C catalyst in Figure 4a. To confirm existence of the CoMoC_yO_z phase, XRD measurements were performed on Mo_2C and $\text{Co-Mo}_2\text{C}$. The XRD results, found in the Supporting Information, indicate a change in the structure of $\text{Co-Mo}_2\text{C}$ upon reduction and the formation of the CoMoC_yO_z phase. Together, the XANES and XRD observations indicate that a highly stable CoMoC_yO_z phase is formed, which is most likely responsible for the enhanced catalytic performance for CO_2 conversion.

In summary, our findings clearly show that Mo_2C is an active catalyst for CO_2 conversion by H_2 , while modifying the catalyst with Co forms a complex with Mo_2C that further improves the activity, selectivity and stability of the catalyst. The active phase of Mo_2C is primarily the carbide phase, as shown by TPSR experiments, but the oxide is generally present throughout the reaction, as indicated by AP-XPS and XANES experiments. The ability of Mo_2C to break the C=O bond, as well as to dissociate hydrogen to either perform hydrogenation of CO_2 or remove oxygen from $\text{Mo}_2\text{C-O}$, makes it dual functional and ideal for CO_2 activation. Furthermore, because Mo_2C is made from much more abundant elements than precious metals, the catalyst can be manufactured at much lower cost, which is critical for achieving a substantial reduction of CO_2 levels by large-scale CO_2 catalytic conversion processes. Furthermore, the reduction of CO_2 also requires parallel advancement in the development of low-cost processes for CO_2 -free H_2 production, such as in electrolysis or photoelectrochemical conversion of H_2O .

Experimental Section

AP-XPS and TPSR experiments were performed by oxidizing a $\text{Mo}(110)$ surface under 1×10^{-6} Torr O_2 at 700 K for 15 min to form MoO_x . The Mo_2C was prepared by a procedure previously described^[30] by exposing $\text{Mo}(110)$ to 5×10^{-7} Torr C_2H_4 at 700 K followed by annealing to 1000 K. After preparation, the sample was moved to the entrance of the XPS analyzer and a total of 800 mTorr gases (100 mTorr CO_2 and 700 mTorr H_2) were leaked into the main chamber at 300 K. Then, the sample was heated to 523 K. After reaction, the sample was cooled in the CO_2/H_2 gas mixture. The reaction products (intensities of ions with m/e of 44, 31, 28, 18 and 15) were recorded with time. The surface species were examined by AP-XPS. The O1s and C1s peaks were measured under the photon energy of 706 eV and 538 eV, respectively. All of the reported binding energies were calibrated by the $\text{Au}4f_{7/2}$ peak of a gold foil at 84.0 eV.

Monometallic and bimetallic catalysts were synthesized by incipient wetness impregnation over as-is commercially obtained CeO_2 ($35\text{--}45 \text{ m}^2 \text{g}^{-1}$, cubic, Sigma-Aldrich) support. Mo_2C was synthesized in a procedure adapted from Shi et al.^[31] BET analysis showed that the synthesized Mo_2C had a surface area of ca. $24.5 \text{ m}^2 \text{g}^{-1}$. Cobalt metal was impregnated onto the Mo_2C through evaporation-deposition of $\text{Co}(\text{NO}_3)_2 \cdot 6\text{H}_2\text{O}$ (Alfa Aesar). Pulse CO chemisorption was performed using an AMI-200ip (Altamira) to compare the number of active sites in each $\text{Co-Mo}_2\text{C}$ catalyst.

EXAFS measurements were used to confirm the structure of Mo_2C , while XANES measurements confirmed the oxidation state of Mo_2C . Mo K-edge spectra were recorded for Mo_2C and 7.5 wt% $\text{Co-Mo}_2\text{C}$.

Mo₂C under the same procedure in a custom designed, in-situ glassy carbon cell. Initial spectra were recorded at room temperature and after reduction in H₂ and He at 723 K. Following reduction, the sample was treated with a CO₂ and H₂ gas mixture, then pure CO₂. During each gas treatment, the glassy carbon cell was heated at 573 K for 90 min, and then cooled to room temperature before XANES spectra were collected. The spectra from each treatment condition was fitted by a linear combination of MoO₃ and Mo₂C standards.

Reactor studies of powder catalysts were carried out in a quartz U-tube reactor under atmospheric pressure. In each experiment, approximately 100 mg catalyst (60–80 mesh) was loaded into the flow reactor. Prior to reaction, the catalyst was reduced under a 1:1 hydrogen and helium mixture (50 mL min⁻¹ total flow) at 723 K for 1 h. For each reaction, CO₂ and hydrogen were set at 20 mL min⁻¹ and 40 mL min⁻¹, respectively. For each experiment, the temperature was ramped to 573 K and held steady for approximately 8 h. In the case of stability studies, the temperature was held constant for 36 h. Product streams were analyzed by online gas chromatography equipped with a flame ionization detector (FID) and thermal conductivity detector (TCD). The concentration of each gas-phase species was calibrated by correlating the peak area of the pure compound to its concentration in a standard calibration gas.

Received: April 8, 2014

Revised: May 2, 2014

Published online: May 19, 2014

Keywords: cobalt · CO₂ Conversion · heterogeneous catalysis · molybdenum carbide · XANES

- [1] U.E.I. Administration, International Energy Outlook 2013, Washington DC, **2013**; <http://www.eia.gov/forecasts/ieo/pdf/0484%282013%29.pdf>.
- [2] T. R. Knutson, R. E. Tuleya, *J. Clim.* **2004**, *17*, 3477–3495.
- [3] J. Hansen, M. Sato, R. Ruedy, K. Lo, D. W. Lea, M. Medina-Elizade, *Proc. Natl. Acad. Sci. USA* **2006**, *103*, 14288–14293.
- [4] M. Uibu, M. Uus, R. Kuusik, *J. Environ. Manage.* **2009**, *90*, 1253–1260.
- [5] S. E. Strand, G. Benford, *Environ. Sci. Technol.* **2009**, *43*, 1000–1007.
- [6] W. Wang, S. P. Wang, X. B. Ma, J. L. Gong, *Chem. Soc. Rev.* **2011**, *40*, 3703–3727.
- [7] G. Centi, S. Perathoner, *Catal. Today* **2009**, *148*, 191–205.
- [8] A. V. Boix, M. A. Ulla, J. O. Petunchi, *J. Catal.* **1996**, *162*, 239–249.
- [9] S. Alayoglu, S. K. Beaumont, F. Zheng, V. V. Pushkarev, H. M. Zheng, V. Iablokov, Z. Liu, J. H. Guo, N. Kruse, G. A. Somorjai, *Top. Catal.* **2011**, *54*, 778–785.
- [10] C. S. Chen, W. H. Cheng, S. S. Lin, *Catal. Lett.* **2000**, *68*, 45–48.
- [11] W. C. Conner, J. L. Falconer, *Chem. Rev.* **1995**, *95*, 759–788.
- [12] M. D. Porosoff, J. G. Chen, *J. Catal.* **2013**, *301*, 30–37.
- [13] T. Staudt, Y. Lykhach, N. Tsud, T. Skala, K. C. Prince, V. Matolin, J. Libuda, *J. Catal.* **2010**, *275*, 181–185.
- [14] J. B. Claridge, A. P. E. York, A. J. Brungs, C. Marquez-Alvarez, J. Sloan, S. C. Tsang, M. L. H. Green, *J. Catal.* **1998**, *180*, 85–100.
- [15] K. Oshikawa, M. Nagai, S. Omi, *J. Phys. Chem. B* **2001**, *105*, 9124–9131.
- [16] P. M. Patterson, T. K. Das, B. H. Davis, *Appl. Catal. A* **2003**, *251*, 449–455.
- [17] P. Liu, J. A. Rodriguez, *J. Phys. Chem. B* **2006**, *110*, 19418–19425.
- [18] N. M. Schweitzer, J. A. Schaidle, O. K. Ezekoye, X. Pan, S. Linic, L. T. Thompson, *J. Am. Chem. Soc.* **2011**, *133*, 2378–2381.
- [19] L. K. Ono, D. Sudfeld, B. Roldan Cuenya, *Surf. Sci.* **2006**, *600*, 5041–5050.
- [20] K.-Z. Qi, G.-C. Wang, W.-J. Zheng, *Surf. Sci.* **2013**, *614*, 53–63.
- [21] P. Liu, J. A. Rodriguez, *J. Chem. Phys.* **2004**, *120*, 5414–5423.
- [22] J. G. Chen, *Chem. Rev.* **1996**, *96*, 1477–1498.
- [23] C. deLeitenburg, A. Trovarelli, J. Kaspar, *J. Catal.* **1997**, *166*, 98–107.
- [24] X. Deng, A. Verdager, T. Herranz, C. Weis, H. Bluhm, M. Salmeron, *Langmuir* **2008**, *24*, 9474–9478.
- [25] A. Goguet, F. C. Meunier, D. Tibiletti, J. P. Breen, R. Burch, *J. Phys. Chem. B* **2004**, *108*, 20240–20246.
- [26] J. H. Bitter, K. Seshan, J. A. Lercher, *J. Catal.* **1998**, *176*, 93–101.
- [27] E. Novák, K. Fodor, T. Szailer, A. Oszko, A. Erdohelyi, *Top. Catal.* **2002**, *20*, 107–117.
- [28] H. Ren, W. Yu, M. Saliccioli, Y. Chen, Y. Huang, K. Xiong, D. G. Vlachos, J. G. Chen, *ChemSusChem* **2013**, *6*, 798–801.
- [29] S. Izhar, H. Kanesugi, H. Tominaga, M. Nagai, *Appl. Catal. A* **2007**, *317*, 82–90.
- [30] H. H. Hwu, J. G. Chen, *Surf. Sci.* **2003**, *536*, 75–87.
- [31] C. Shi, A. J. Zhang, X. S. Li, S. H. Zhang, A. M. Zhu, Y. F. Ma, C. T. Au, *Appl. Catal. A* **2012**, *431*, 164–170.